Applied Surface Science 351 (2015) 1204–1212

Contents lists available at ScienceDirect

Applied Surface Science

journal homepage: www.elsevier.com/locate/apsusc

A novel silanized $CoFe_2O_4$/fluorinated waterborne polyurethane pressure sensitive adhesive

Heqing Fu*, Yin Wang, Weifeng Chen, Wei Zhou, Jing Xiao

School of Chemistry and Chemical Engineering, South China University of Technology, Guangzhou 510640, China

ARTICLE INFO

Article history:
Received 14 April 2015
Received in revised form 15 June 2015
Accepted 19 June 2015
Available online 25 June 2015

Keywords:
Thermal stability
Hydrophobicity
Dynamic mechanical properties
Adhesive properties

ABSTRACT

A novel silanized $CoFe_2O_4$/fluorinated waterborne polyurethane (SC/FWPU) pressure sensitive adhesive was synthesized and characterized by atomic force microscopy (AFM), thermogravimetric analysis (TGA), dynamic mechanical analysis (DMA) and contact angle tester. The adhesive properties were measured in a test machine. Experimental results showed that the hydrophobicity, thermal stability, dynamic mechanical properties, as well as adhesive properties of SC/FWPU were improved with the incorporation of SC into FWPU. The dynamic hydrophobicity can be well described by the wetting kinetic model. The spreading-penetration parameter increased with an increase in SC content. The higher the spreading-penetration parameter is, the faster the contact angle reaches equilibrium, and the faster the SC/FWPU pressure sensitive adhesive penetrates and spreads.

1. Introduction

The solvent-borne pressure sensitive adhesive has been widely used in industry due to the excellent adhesive strength, water resistance and thermal stability. However, its use in the nonpolar film is restricted as it emits volatile organic compound (VOC) and causes problems like toxicity, flammability and pollution. To overcome these problems, waterborne polyurethane (WPU) pressure sensitive adhesive has been developed for use in the nonpolar films field [1]. However, due to the poor wettability, heat resistance, and water resistance, the waterborne polyurethane pressure sensitive adhesive needs to be modified to ensure its application in the nonpolar film field.

In order to improve the wettability, the waterborne polyurethane pressure sensitive adhesive should be modified to decrease the surface energy. Introducing fluorine into polyurethane chain was reported to be an effective method to lower the surface energy and improve surface properties as fluorine has quite low surface energy [2,3]. On the other hand, high heat resistance is required for pressure sensitive adhesive when used in food packaging. WPU is a type of linear thermoplastic structure polymers that contains hydrophilic groups in the molecular chain with no cross-linking structure, therefore its heat resistance is poor and needs to be modified [4,5]. Inorganic nanomaterial modification is an effective method to enhance the heat resistance and mechanical property of WPU film [7–11]. Nano-$CoFe_2O_4$ can improve the thermal, mechanical and hydrophobicity of polymers. However, $CoFe_2O_4$ is incompatible with polymer matrix, it needs to be modified. The organic modification of $CoFe_2O_4$ is extremely important for preparing $CoFe_2O_4$-polymer nanocomposites. Grafting organosilane on the surface of $CoFe_2O_4$ can effectively improve its dispersion in polymers by increasing the interfacial compatibility. Moreover, the amino groups grafted on the surface of $CoFe_2O_4$ can react with PU prepolymer and participate in the polymerization reaction, which guarantees a durable chemical junction between $CoFe_2O_4$ and polyurethane in the two incompatible phases. In this work, perfluoroalkyl ether diamine was selected as chain extender, and fluorine atom and silanized $CoFe_2O_4$ (SC) were introduced into polyurethane chain. The effects of SC on the surface morphology, thermal stability, dynamic mechanical properties and hydrophobicity of SC/FWPU films were investigated. According to the adsorption and diffusion theory, good wettability is essential to provide close contact between two substrates. Dynamic hydrophobicity process is analyzed by the contact angles (maximum/advancing) with time. The spreading–penetration parameter (K) was calculated. The dynamic wettability model was developed to describe the hydrophobicity process and reveal the relationship between wettability and adhesive properties of the SC/FWPU adhesive to the nonpolar polyolefin film. Moreover, the influence of SC on the adhesion properties of SC/FWPU PSA was discussed.

* Corresponding author. Tel.: +86 020 87114919; fax: +86 020 87112047.
E-mail address: fuhq@scut.edu.cn (H. Fu).

http://dx.doi.org/10.1016/j.apsusc.2015.06.121
0169-4332/

2. Experimental

2.1. Materials

Isophorone diisocyanate (IPDI), 1,4-butylene adipate glycol (PBA, Mn = 2000) and acetone were supplied by Donghao Resine Co. Ltd., China. $CoFe_2O_4$ was purchased from Hubei Gaozhi Chemical Agent Co. Ltd., China. 3-Aminopropyltriethoxysilane (APTES) and ethanol were supplied by Aladdin, China. Dimethylol propionic acid (DMPA) was supplied by Perstop, Sweden. Dibutyltin dilaurate (DBTDL), n-methyl pyrrolidone (NMP) and triethylamine (TEA) were supplied by Shanghai Lingfeng Chemical Agent Co. Ltd., China. perfluoroalkyl ether diamine was purchased from Guangzhou Co., Ltd. Cast polypropylene film (CPP) was supplied by Shenzhen Hengfeng Packaging Materials Co., Ltd.

2.2. Preparation of silanized $CoFe_2O_4$

5.0 g of $CoFe_2O_4$ was dispersed in 200 mL of hydroalcoholic solution (25/75 by volume), and 10 mL of APTES was then added into the mixture, and stirred for 30 min in a 200 mL flask. The mixture was then refluxed with electromagnetic stirring at 60 °C for 12 h. Finally, the $CoFe_2O_4$ was separated by filtration and the solid was washed by excess of amount ethanol and deionized water for three times. The silanized $CoFe_2O_4$ (SC) was obtained after dried at room temperature in vacuum overnight.

2.3. Preparation of silanized $CoFe_2O_4$/fluorinated waterborne polyurethane

The silanized $CoFe_2O_4$/fluorinated waterborne polyurethane (SC/FWPU) were prepared by a prepolymer process. A dry 1000 mL four-necked glass reaction kettle equipped with a mechanical stirrer, thermometer, condenser and a nitrogen inlet was placed in a water bath. The stoichiometric PBA was dried at 110 °C for 1.5 h in a vacuum oven, IPDI, DMPA and the catalyst DBTDL were added into the reactor under N_2 atmosphere, and the reaction was carried out at 80 °C for 2 h. After that, 5 wt% of perfluoroalkyl ether diamine dissolved in NMP was added into the kettle where the reaction temperature was set as 75 °C. Then, silanized $CoFe_2O_4$ (in weight fraction of 1, 2, 3, 4 wt%) was added into the reactor and reacted for 2 h. The reaction proceeded until the residual NCO reached the expected content (determined by the standard dibutylamine back-titration method [12]). After the prepolymer was cooled to 50 °C, the carboxylic acid in the prepolymer was neutralized by TEA solution for 30 min at 40 °C to obtain ionomer. The ionomer was dispersed into the stoichiometric amount of deionized water under vigorous stirring. The SC/FWPU with a solid content of 40 wt% was obtained after removing the acetone by vacuum distillation.

2.4. Film preparation

The SC/FWPU films were prepared by casting the SC/FWPU on a PTFE mould dried at room temperature for 7 days. Then the films were placed in a vacuum oven at 60 °C for 24 h before characterization.

2.5. Characterization

The thermogravimetric analysis (TGA) was performed by STGA 449C (Netzsch, Germany) with a heating rate of 5 °C/min, 10 °C/min, 15 °C/min and 20 °C/min from 50 to 600 °C under a N_2 atmosphere respectively.

The atomic force microscopy (AFM) measurement was performed on CSPM 2003 with 10 μm × 10 μm scan area and the images were acquired under ambient conditions in tapping mode using a nanoprobe cantilever.

The contact angle and surface tension were measured by the JC2000C1 using the sessile-drop method at 25 °C [13].

Advancing contact angles were measured after sequential deposition with a small syringe and needle. A small drop of water was deposited on the surface, and then additional water was added to advance the contact line. The needle was inserted into the drop during injection to prevent drops from moving on the film surface. For receding contact angles, water was withdrawn until the contact line retracted [14]. Measurements were made on the film surface of more than five droplets and averaged. The dynamic contact angle was determined by JC2000C1 contact angle measuring instrument. The determination of balance contact angle was taken at 10 s after glue dropping and gradually spreading on the film surface.

Dynamic mechanical analysis (DMA) was analyzed by the DMA 242C (Netzsch, Germany) under the tension mode from −100 to 120 °C with a frequency of 1 Hz and a heating rate of 2 °C/min. The size of specimen was 25 mm × 6 mm × 1 mm.

Differential scanning calorimetry (DSC) was performed on a thermal analyzer (Netzsch DSC200 F3, Germany). 3–5 mg of samples was heated up to 150 °C to move the thermal history. Then, the samples were cooled to −70 °C, and the non-isothermal measurement was scanned from −70 to 100 °C. The rate of heating and cooling was 10 °C/min.

Tack was studied as a function of ball tack obtained from the stainless steel ball test. Diameters of stainless steel balls used were varied from 1/32 in. (No. 1) to 32/32 in. (No. 32). Ball tack was defined as the highest ball number attached to the sample surface.

180° peels strength was measured using Instron tension meter Model 3367. The specimen for 180° peel strength test was cut into a tape strip (25 mm × 100 mm corona-treated polypropylene films), which is boned to a horizontal target substrate surface of a clean steel test plate, and then 2 kg standard roller was passed four times to press onto the tape strip to make the contact. After keeping the specimen at room temperature for 24 h,the tape's free end was clamped to the upper jaw and the steel test plate was clamped to the under jaw of the Instron tension meter, which pulled the tape at an angle of 180° at a constant speed of 300 mm/min at room temperature. The value of 180° peel strength was an average of five specimens.

Shear resistance was measured using holding power shear tester. A strip of 25 mm × 25 mm adhesive tape was applied to a stainless steel surface mounted in a vertical position after which a 500 g weight was attached to the tape. The time to slip completely was recorded as failure time.

3. Results and discussion

3.1. Effect of the SC on the surface morphology of the SC/FWPU film

The surface morphology of the SC/FWPU film was characterized by AFM. Fig. 1 shows the 3D AFM images of pure WPU film and the SC/FWPU film. The results of preliminary quantitative analysis, including root-mean-square roughness (rms, which gives the standard deviation of the height values), surface roughness factor (R, $R = 1 + S_{dr}$, S_{dr} is surface area ratio, which is the ratio between the interfacial and projected areas) and mean roughness (Ra, which is the average deviation of the peaks and valleys from the mean elevation), were obtained. The results of preliminary are shown in Table 1. The surface morphology of WPU film is smooth (Fig. 1a), with the roughness average (Ra) of 4.88 nm, root-mean-square (rms) of 6.24 nm, roughness factor (R) of 1.1 (Table 1). In the case of SC/FWPU film structures, some discontinuous regions with

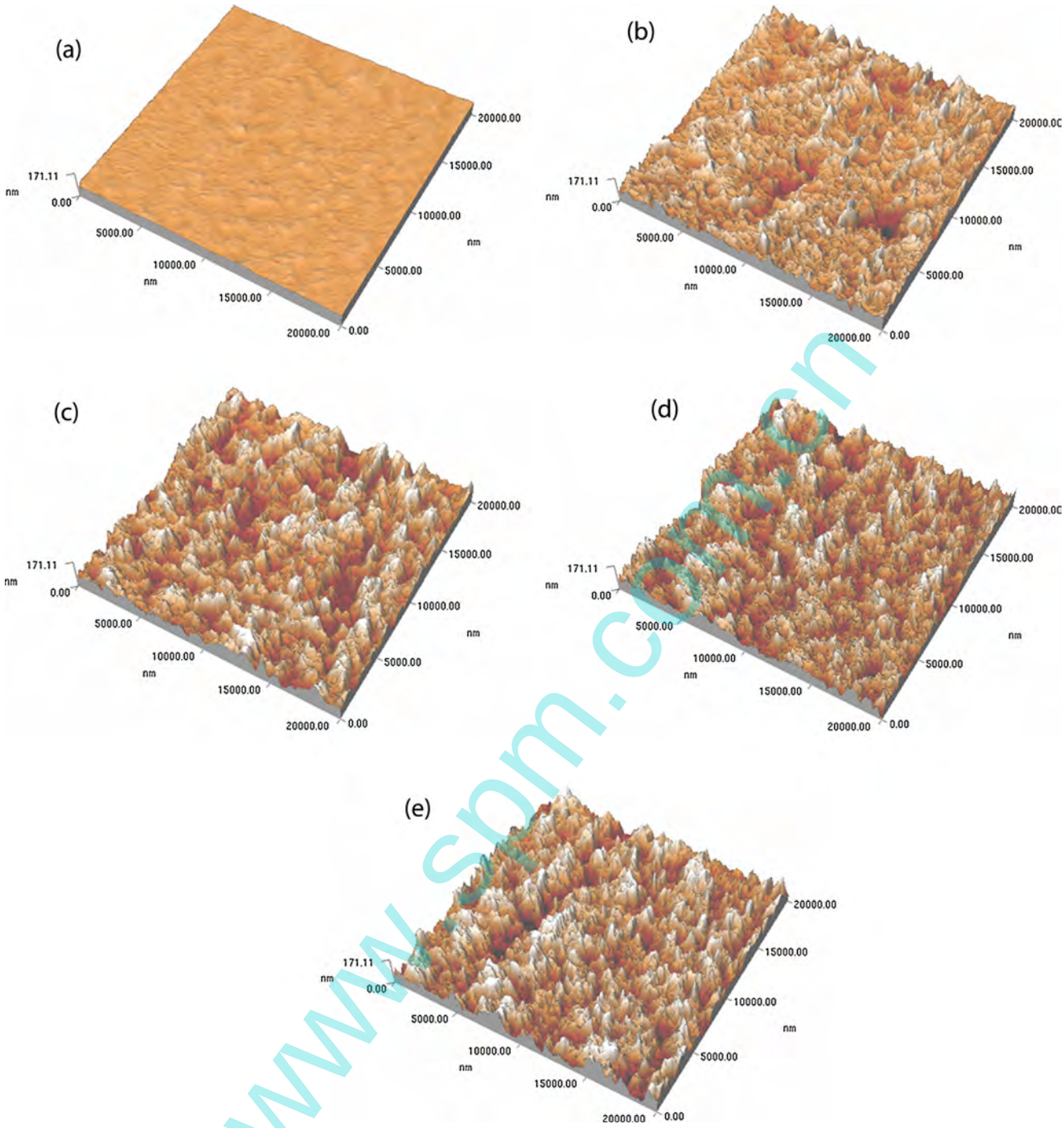

Fig. 1. Three-dimensional images of SC/FWPU: (a) FWPU (b) SC-1/FWPU (c) SC-2/FWPU (d) SC-3/FWPU and (e) SC-4/FWPU.

Table 1
Effect of the SC content on the surface morphology of the SC/FWPU film.

Samples	Ra (nm)	Sq (nm)	R_0
FWPU	4.88	6.24	1.1
SC-1/FWPU	15.6	19.6	1.4
SC-2/FWPU	22.2	28.1	1.8
SC-3/FWPU	31.8	40.1	2.6
SC-4/FWPU	40.0	51.1	3.1

relatively bright and dark parts were observed (Fig. 1b–d). The bright regions in AFM images represents the SC phase, while the dark regions represents the polyurethane phase. Increasing the SC content showed a more distinct microphase separated structure, and more SC particle enriched on the surface of SC/FWPU film. And the roughness average (Ra) increased from 15.6 nm to 40 nm with increasing SC content, so as the root-mean-square (rms) value and roughness factor (R) value.

The improvement of surface roughness could be attributed to the existence of SC particles, which were uniformly distributed

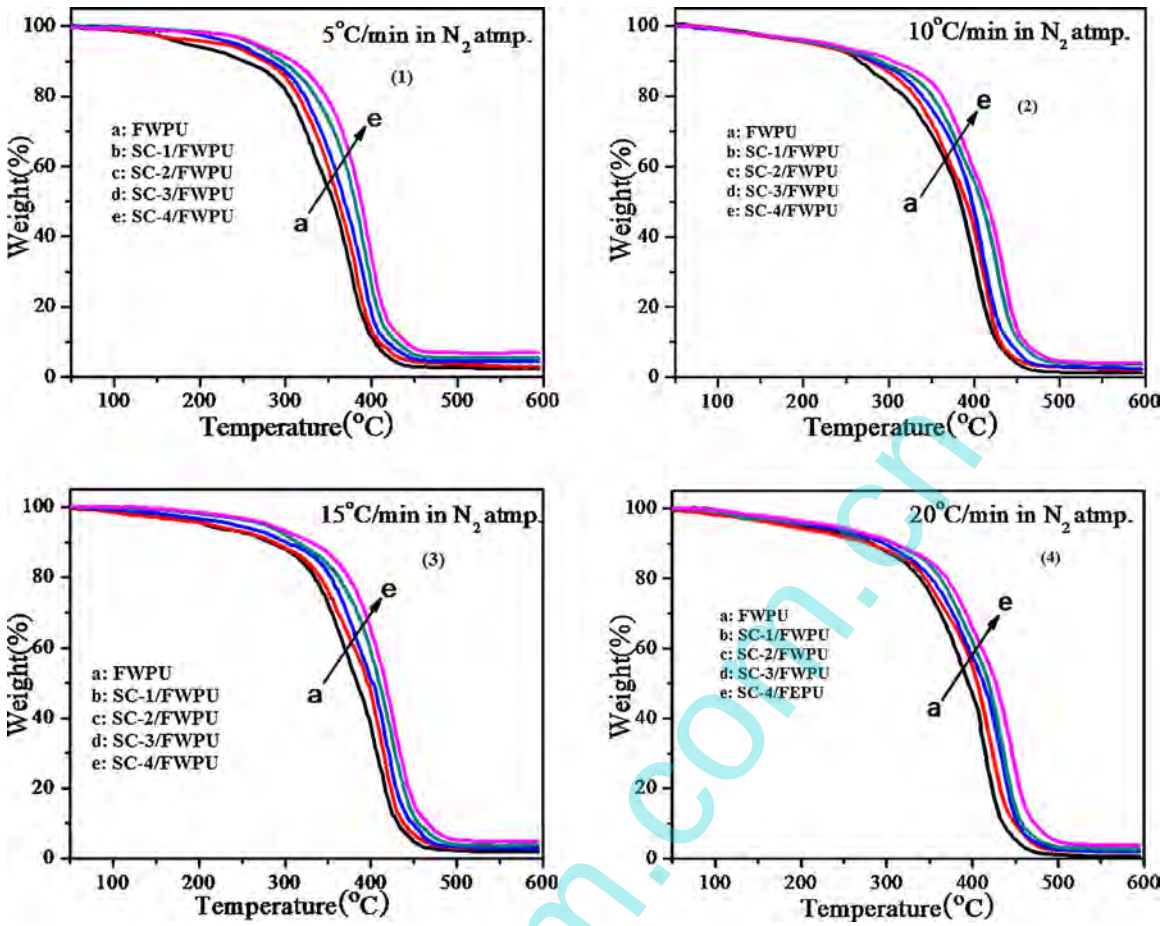

Fig. 2. TG curves for SC/FWPU composites with different SC content at different heating rates.

in the FWPU matrix. Moreover, with the increasing of nanofillers content, SC particles immigrate to the surface of FWPU, which effectively improved the surface roughness of SC/FWPU.

3.2. Effect of the SC content on the thermal stability of SC/FWPU film

Fig. 2 shows the TGA curves of SC/FWPU film with different SC content at different heating rates. As Fig. 2(a) shows, the weight loss up to 150 °C is due to the evaporation of residual moisture present in the films. The weight loss in the range 250–350 °C is attributed to the dissociation of urethane bonds to form isocyanates, alcohol, amine and CO_2 [15]. The degradation in the range 350–500 °C is due to the scission of PBA. All the film samples show two-stage decomposition temperatures, and the fraction of decomposed soft segments is about 60%, which is basically consistent with the amount of soft segments in recipe. The thermogravimetric data for the SC/FWPU films is listed in Table 2.

The degradation temperature in the first stage (T_{max1}) and in the second stage (T_{max2}) increased with an increase in the heating rate of degradation process, suggesting SC/FWPU films are more thermally stable at higher heating rate. On the other hand, the degradation temperature of the SC/FWPU films increased with an increase in the SC content. This was because the inorganic particles were uniformly distributed in polymer matrix acted as thermal barriers, which greatly improved the thermal stability of SC/FWPU films. Moreover, amine groups on the surfaces of SC reacted with polyurethane prepolymer resulted the increase of cross-linking density with an increase in the SC content. The higher crosslinking yields higher degradation temperature, thus higher thermal stability of SC/FWPU film.

In order to further investigate the effect of SC content on the thermal stability of SC/FWPU film, the activation energy for the decomposition process of SC/FWPU film was calculated by the Kissinger method using the following equation [16].

$$\ln\left(\frac{\beta}{T_{max}^2}\right) = -\frac{E_a}{RT_{max}} + \left\{\ln\frac{AR}{E_a} + \ln[n(1-\alpha_{max})^{n-1}]\right\} \quad (1)$$

where β is heating rate, T_{max} is temperature corresponding to the maximum degradation, A is pre-exponential factor, E_a is activation energy, α_{max} is maximum conversion, n is order of the reaction, and R is the universal gas constant. A plot of $\ln(\beta/T_{max}^2)$ versus $1/T_{max}$ will give a straight line with the slope being $-E_a/R$. The calculated activation energies (E_a) for the SC/FWPU film were given in Table 3. Fig. 3 showed the Kissinger plots for the SC/FWPU composites at two different stages. From Fig. 3 it was found that with increasing SC content from 0 to 2 wt%, the calculated activation energies (E_a) increased from 95.18 to 141.38 kJ/mol, from 108.2 to 139.08 kJ/mol at T_{max1} and at T_{max2}, respectively. This is due to the increasing of crosslinking between the waterborne polyurethane and SC. The more of the SC content, the higher the crosslinking between the polyurethane and SC, and the higher the thermal stability of the SC/FWPU film was obtained. The increased activation energy values proved that SC promoted that the incorporated thermal stability of the SC/FWPU nanocomposites.

Table 2
Thermogravimetric data for the SC/FWPU films.

Samples	First stage degradation temperature T_{max1} (°C) at different heating rates (°C/min)				Second stage degradation temperature T_{max2} (°C) at different heating rates (°C/min)			
	5	10	15	20	5	10	15	20
FWPU	301	322	327	336	374	391	409	415
SC-1/FWPU	310	331	336	344	380	400	408	422
SC-2/FWPU	320	340	348	351	393	405	418	432
SC-3/FWPU	331	345	354	363	396	420	426	434
SC-4/FWPU	342	357	360	373	405	424	432	443

Table 3
The calculated activation energy of the SC/FWPU film.

Samples	First stage degradation, T_{max1} (°C)			Second stage degradation, T_{max2} (°C)		
	Slope	E_a (kJ/mol)	Correlation coefficient (r^2)	Slope	E_a (kJ/mol)	Correlation coefficient (r^2)
FWPU	−11,447	95.18	0.9624	−12,991	108.01	0.9821
SC-1/FWPU	−13,455	111.87	0.9702	−14,068	116.97	0.9801
SC-2/FWPU	−14,443	120.09	0.9643	−15,055	125.17	0.9448
SC-3/FWPU	−15,633	129.98	0.9722	−15,705	130.58	0.9604
SC-4/FWPU	−17,004	141.38	0.9409	−16,727	139.08	0.9914

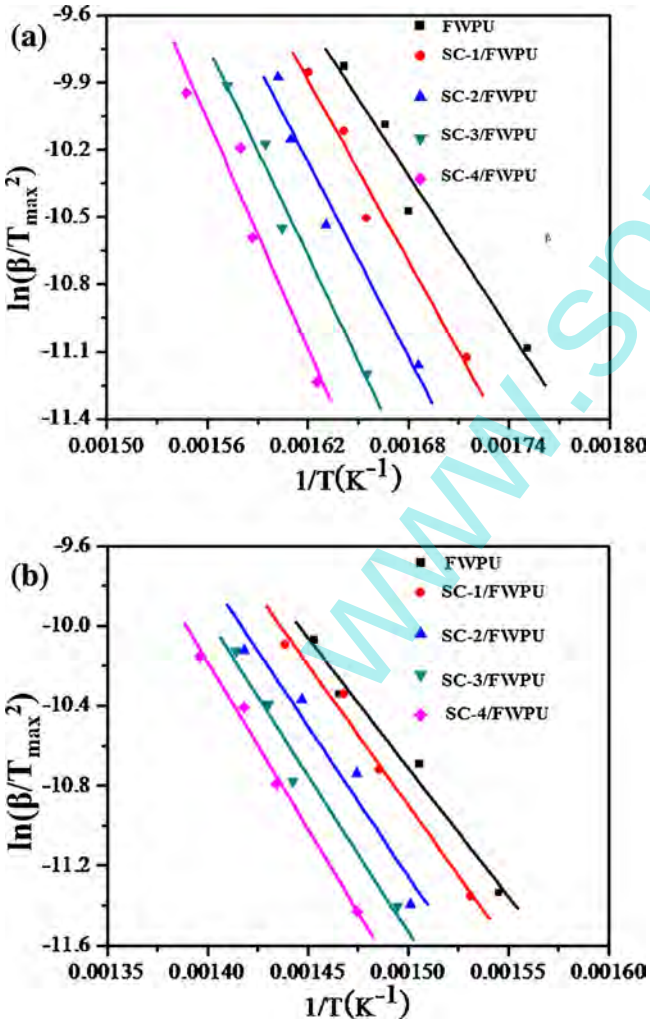

Fig. 3. Kissinger plots for the SC/FWPU film at two different stages: (a) T_{max1} and (b) T_{max2}.

3.3. Effect of SC content on the static hydrophobicity of SC/FWPU film

The static hydrophobicity of SC/FWPU film was investigated by measuring the static contact angle and the surface free energy. The surface free energy of SC/FWPU film was also calculated using Owens–Went equation and Wu equation. Owens–Went equation [17] is based on the Bethelot hypothesis. Their assumption was that the value of the surface tension γ_s is the sum of the dispersive interaction component γ_s^d, and the polar interaction component, γ_s^p. The solid–liquid interfacial tension was assumed to be given by:

$$\gamma_s = \gamma_s^d + \gamma_s^p \quad (1)$$

To calculate the interfacial tension between polymers or between a polymer and an ordinary liquid, Wu propose an equation based on "reciprocal" mean and force additivity:

$$\gamma_{12} = \gamma_1 + \gamma_2 - \frac{4\gamma_1^d\gamma_2^d}{\gamma_1^d\gamma_2^d} - \frac{4\gamma_1^p\gamma_2^p}{\gamma_1^p\gamma_2^p} \quad (2)$$

where γ_{12} is the interfacial tension, γ_1, γ_1^d, γ_1^p is the surface tension, dispersive component and polar component of water (γ_1^d = 21.8 mJ m^{-2}, γ_1^p = 51.0 mJ m^{-2}) [17], γ_2, γ_2^d, γ_2^p is the surface tension, dispersive component and polar component of ethylene glycol (γ_2^d = 29.3 mJ m^{-2}, γ_2^p = 19.0 mJ m^{-2}) [18], respectively.

Eq. (2) appears to predict accurately the interfacial tension between polymers or between a polymer and an ordinary liquid, where, Fowkes equation becomes non-applicable. Eq. (2) can also be used to calculate the surface free energy and polarity of polymers or organic solids from contact angle.

Combination of Eq. (2), Young equation and Owens–Went equation lead to:

$$(1+\cos\theta_1)\gamma_1 = 4\left(\frac{\gamma_1^d\gamma_s^d}{\gamma_1^d+\gamma_s^d} + \frac{\gamma_1^p\gamma_s^p}{\gamma_1^p+\gamma_s^p}\right) \quad (3)$$

$$(1+\cos\theta_2)\gamma_2 = 4\left(\frac{\gamma_2^d\gamma_s^d}{\gamma_2^d+\gamma_s^d} + \frac{\gamma_2^p\gamma_s^p}{\gamma_2^p+\gamma_s^p}\right) \quad (4)$$

where θ_1 and θ_2 are the equilibrium contact angles of water and ethylene glycol on the surface of SC/FWPU film, respectively.

Eqs. (2)–(4) allow calculation of the surface energy.

The static contact angle and surface free energy values are shown in Table 4. The static water contact angle increased from 71.3° to 91.3° with increasing SC content. This is because that the

Table 4
Effect of SC content on the static contact angle and surface free energy of the SC/FWPU film.

Samples	Content angle (°)		Surface free energy (mJ/m^2)		
	Water	Ethylene glycol	γ_s^d	γ_s^p	γ_s
FWPU	71.3	50.5	15.7	17.1	32.8
SC-1/FWPU	76.7	59.8	12.2	15.9	28.1
SC-2/FWPU	81.4	67.5	9.4	14.9	24.3
SC-3/FWPU	93.2	74.6	14.0	5.6	19.6
SC-4/FWPU	94.3	75.7	13.9	5.2	19.1

Table 5
Effect of SC content on advancing contact angle, receding contact angle and contact angle hysteresis of the SC/FWPU film.

Samples	θ_A (°)	θ_R (°)	$\Delta\theta$ (°)
FWPU	97.3	78.9	18.4
SC-1/FWPU	100.3	75.5	24.8
SC-2/FWPU	105.5	72.4	33.1
SC-3/FWPU	114.2	70.8	43.4
SC-4/FWPU	118.3	102.1	16.2

SC nanoparticles with hydrophobicity were uniformly dispersed in polymer matrix and immigrated to the surface of FWPU, which improved the hydrophobicity of the polyurethane film. Moreover, film formed water repellant surface after the Si–O–Si network structure was introduced to the polyurethane, which was beneficial to enhance the static contact angle of the SC/FWPU film. On the other hand, when the SC reacted with polyurethane prepolymer, the crosslinking density of polymer nanocomposites was enhanced. Therefore, the surface properties of SC/FWPU film were improved with the increase of SC content.

3.4. Effect of SC content on the dynamic hydrophobicity of SC/FWPU film

3.4.1. The advancing contact angle, receding contact angle and contact angle hysteresis of SC/FWPU film

One static contact angle is not sufficient to describe the hydrophobicity of solid film. When a liquid drop is placed on a solid surface, it spreads until it attains an equilibrium state. If additional liquid is added to the drop, the contact line advances and stops. Each time motion ceases, the drop exhibits an advancing contact angle (θ_A). If enough liquid is removed, the contact line retreats. When motion ceases, the drop exhibits a receding contact angle (θ_R). The difference between θ_A and θ_R is referred to as contact angle hysteresis $\Delta\theta$, $\Delta\theta = \theta_A - \theta_R$ [19].

In order to understand the dynamic wettability of SC/FWPU film, the advancing contact angle (θ_A), receding contact angle (θ_R) and contact angle hysteresis ($\Delta\theta$) were measured. Table 5 shows the effect of SC content on advancing contact angle, receding contact angle and contact angle hysteresis of the SC/FWPU film. As clearly seen from Table 5, when the content of SC was 0, advancing contact angle (θ_A) and receding contact angle (θ_R) on SC/FWPU film were 97.3° and 78.9°, respectively. And the advancing contact angle (θ_A) increased with increasing content of SC. The receding contact angle (θ_R) decreased and water contact angle hysteresis ($\Delta\theta$) increased when the content of SC was below 3 wt%. While receding contact angle (θ_R) values increased and water contact angle hysteresis ($\Delta\theta$) decreased when the content of SC was above 4 wt%. This is because the surface roughness of SC/FWPU film increases with the increasing of SC (Table 5). The hydrophobicity is not only governed by the surface energy of the solid material but also by the surface roughness of the solid material. The surface roughness can change the advancing contact angle, receding contact angle and contact angle hysteresis. Two distinct models have been proposed to explain this phenomenon: the Wenzel model and the Cassie model [20,21]. When the content of SC content is below 3 wt%, according to the Wenzel model, the roughness regime in which both advancing contact angle and water contact angle hysteresis increase as roughness factor (R) increases (water penetrates into the surface cavity) [20]. When the content of SC content is above 4 wt%, according to the Cassie model, as roughness factor (R) further increases passing a critical level, the water receding angle also increases dramatically (water does not penetrate into the surface cavity, there is an air pocket between the water droplet and the solid surface), thus minimized the water contact angle hysteresis.

3.4.2. Instantaneous contact angle, equilibrium contact angle and spreading-penetration parameters of SC/FWPU film

The dynamic hydrophobicity is also characterized by instantaneous contact angle, equilibrium contact angle and spreading-penetration parameters. When a liquid drop is placed on the solid surface, the instantaneous (initial) contact angle (θ_i) is formed and expands in the contact area under the surface tension (this process is defined as spreading). Simultaneously, the droplet penetrates into the solid and is gradually absorbed by the solid (this process is defined as penetration). Finally, no spreading and penetration occur. The contact angle at the final time is equilibrium contact angle (θ_e).

A wetting model was developed to describe the dynamic wetting process, in which a parameter (K) was used to quantify the SC/FWPU penetration and spreading during the adhesive wetting process. Both spreading and penetration cause the contact angle changes as a function of time. The contact angle and K value were derived to illustrate kinetics of wetting, and therefore evaluate the dynamic wettability of the SC/FWPU film.

For an ideal liquid–solid systems, spreading and penetration rate as a function of time can be expressed as

$$\frac{d\theta}{dt} = -K\theta \tag{2}$$

in which θ represents contact angle at time, t represents wetting time, K is a constant referred to the intrinsic relative contact angle decrease rate. The physical meaning of the K value represents how fast the liquid spreads and penetrates into the porous structure of material.

When the penetration and diffusion are near to zero, Eq. (2) changes to

$$\frac{d\theta}{dt} = -K\theta\left(1 - \frac{\theta_i - \theta}{\theta_i - \theta_e}\right) \tag{3}$$

where θ_i represents the initial contact angle, θ_e represents equilibrium contact angle.

Solving Eq. (3), we have

$$\theta = \frac{\theta_i \cdot \theta_e}{\theta_i + (\theta_e - \theta_i)\exp[K(\theta_e/(\theta_e - \theta_i))t]} \tag{4}$$

This model was employed to quantify the material penetration performances using the spreading–penetration parameters (K value) as a constant to characterize penetration rate [22]. Reorganizing Eq. (4), we have

$$e^{K(\theta_e/(\theta_e-\theta_i))t} = \frac{\theta_i(\theta_e - \theta)}{\theta(\theta_e - \theta_i)} \tag{5}$$

Logarithmic transformation of the Eq. (5),

$$Kt = \frac{\theta_e - \theta_i}{\theta_e}\ \ln\frac{\theta_i(\theta_e - \theta)}{\theta(\theta_e - \theta_i)} \tag{6}$$

In Eq. (6), $((\theta_e - \theta_i)/\theta_e)\ln(\theta_i(\theta_e - \theta)/\theta(\theta_e - \theta_i))$ is defined as a, then a linear equation was expressed as

$$a = Kt \tag{7}$$

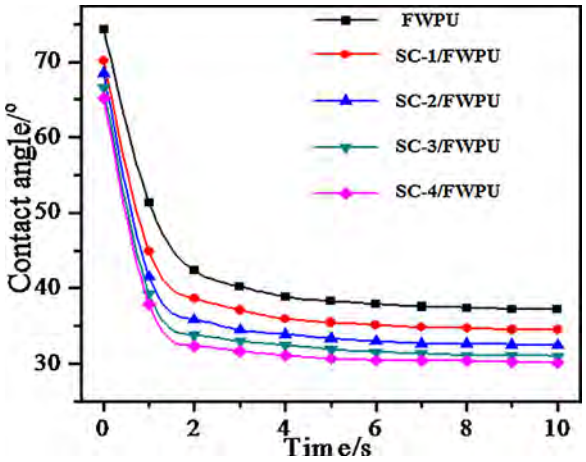

Fig. 4. Contact angle of SC/FWPU with different SC content at different contact time.

Table 6
The value of θ_i, θ_e and K values of the SC/FWPU films.

Samples	Contact angle (°)		K	R^2
	θ_i	θ_e		
SC-0	74.4	37.1	0.5476	0.9905
SC-1	70.2	34.5	0.6440	0.9935
SC-2	68.5	32.4	0.7077	0.9763
SC-3	66.5	31.0	0.7541	0.9885
SC-4	65.2	30.1	0.7841	0.9976

Plot a–t, different slopes of the straight lines are obtained, and the slope is K-value

Fig. 4 shows the evolution of the contact angle of SC/FWPU with different SC content at different contact time. The results showed that the contact angle values decreased with the extension of time. Table 6 lists θ_i, θ_e and K of the SC/FWPU films. It's observed that the initial contact angle θ_i decreased from 74.4° to 65.2°, and equilibrium contact angle θ_e decreased from 37.1° to 30.1° with increasing in SC content. This is because with the increase of SC content, more SC reacted with FPU and formed cross-linked structure, which increased the dynamic hydrophobicity of SC/FWPU film.

According to the Eq. (6), K was calculated as the slope of fitted straight line. Fig. 5 is a–t curve of SC/FWPU with different SC content, θ_i, θ_e and K of the SC/FWPU films were listed in Table 6.

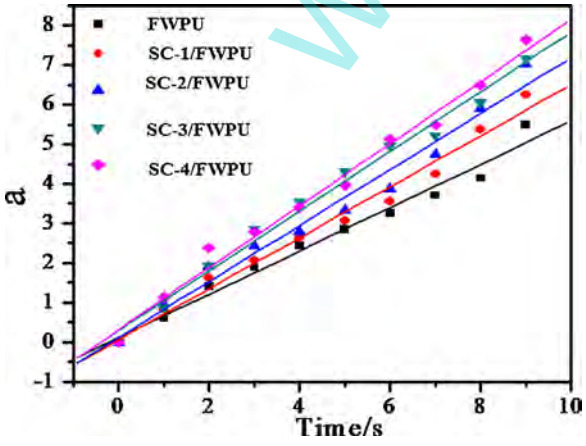

Fig. 5. a–t curve of SC/FWPU with different SC content.

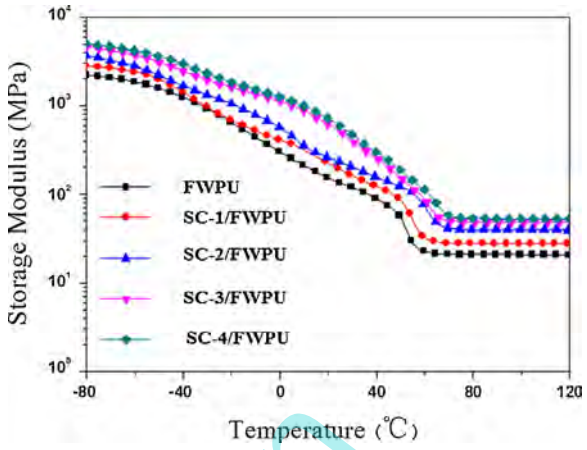

Fig. 6. Storage modulus (G') of the SC/FWPU film with different SC content.

With the increasing SC content, the K value increased. The higher the K value, the faster the contact angle reaches equilibrium, and the faster the liquid penetrates and spreads, which means the spreading–penetration speed of SC/FWPU pressure sensitive adhesive is faster. This is because with the increase of SC content, more SC reacts with polyurethane, and more Si–O–Si network structure was introduced to the fluorinated waterborne polyurethane pressure sensitive adhesive, which decreased the interfacial tension of SC/FWPU pressure sensitive adhesive, resulting in faster spreading–penetration speed and better dynamic hydrophobicity.

3.5. *Effect of SC content on the dynamic mechanical properties of SC/FWPU film*

The incorporation of SC affects the dynamic mechanical properties of the SC/FWPU film. DMA was employed to examine the dynamic mechanical properties of the SC/FWPU film. Storage modulus (G') is plotted against temperature in Fig. 6. SC/FWPU film present high G' with the introduction of SC. G' of SC/FWPU film increases by increasing the SC content, while it decreases by increasing temperature. It is also noted that a slight decrease of E' up to −40 °C was observed in glassy plateau region for SC/FWPU, followed by a decrease of G' for one order of magnitude due to the glass-rubbery transition. And a sharp drop in G' is noted at about 40 °C, associated with the melting of crystalline phase. Above the melting point, G' of polyurethane film modified by the SC is still considerably higher than that of pure polymer. However, the dissipation tends to diminish or even disappear by increasing the SC content. This is because the SC particles acted as crosslinking agent, which enhanced the crosslinking density of SC/FWPU nanocomposties, resulting the stiffer polymer film. The tan δ curves of the SC/FWPU film are presented in Fig. 7. A broad peak with low intensity around −40 °C was observed in the tan δ curve, corresponding to the glass transition temperature (T_g) of the soft segment. With the SC content increased from 0 to 4 wt%, the melting temperature of crystalline phase (T_m) increased from 37.8 °C to 46.3 °C, suggesting that the phase separation between soft segments and hard segments was improved. This could be attributed to the introduced SC nanoparticles, which reacted with polyurethane prepolymer and formed urea groups in the hard segments. Furthermore, the formed urea groups donated more proton than urethane linkage and formed more hydrogen bondings with the remained hydroxyl groups on the surface of SC particles, resulting in increasing the hydrogen bonding interaction and interfacial interaction between inorganic particles and hard microdomains.

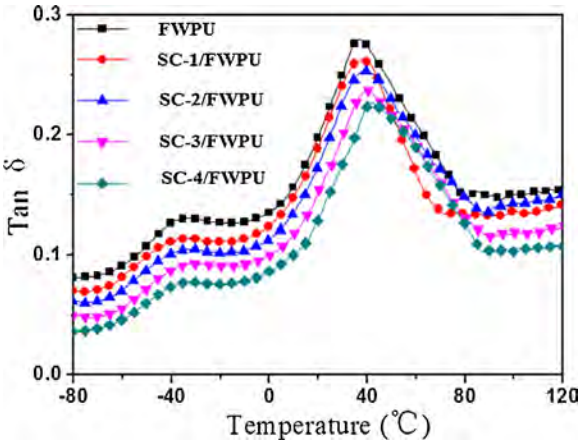

Fig. 7. tan δ curves of the SC/FWPU films with different SC content.

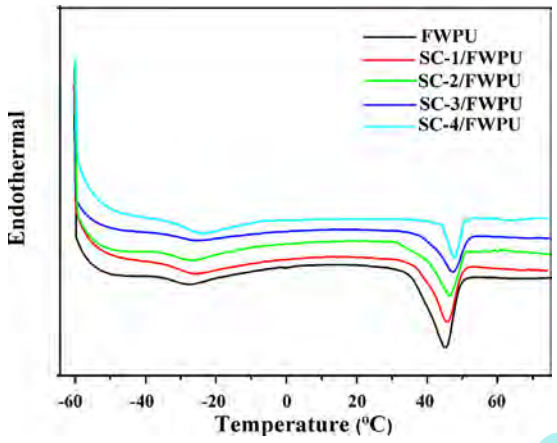

Fig. 8. DSC curves of the SC/FWPU films with different SC content.

3.6. Effect of SC content on the thermal properties of SC/FWPU film

Thermal properties of SC/FWPU films with different SC content were measured by differential scanning calorimetry (DSC) and the results were shown in Fig. 8. It is obvious that the glass transition temperature of soft segments (T_g) appears around −33 °C for all samples, while an endothermic peak corresponded to the melting temperature (T_m) of crystalline phase appears at about 45 °C. With the increase of the SC content from 0 to 4 wt%, the T_m shifted towards a higher temperature from 44.56 to 47.73 °C. This might be attributed to the interaction between the SC particles and polyurethane molecular chains discussed above. Owing to the difference of measuring principles, there is a little difference between the T_g data from DSC and DMA, but the T_g of all samples from DSC are close to each other and the melting temperature of crystalline phase increased with the increase of SC content, which are consistent with the results of DMA.

3.7. Adhesion properties of SC/FWPU PSA

The adhesive properties of SC/FWPU PSA were characterized by Tack, 180° peel strength and Shear resistance. Table 7 listed the effect of SC content on the Tack, 180° peel strength and Shear resistance. From Table 7, it was found that with the increase of SC content, tack and 180° peel strength reduced significantly, and the shear resistance increased. This is because by increasing SC content, the amount of SC reacted with polyurethane increased, and the crosslinking degree of SC/FWPU PSA increased, causing a more compact structure and a decreased tack and 180° peel strength, and increased shear resistance.

Table 7
The effect of SC content on the tack, peel strength and shear resistance.

Samples	Tack (No*)	180° peel strength (N.25 mm^{-1})	Shear resistance (h)
FWPU	18	18.5	22
SC-1/FWPU	16	15.6	33
SC-2/FWPU	12	12.1	52
SC-3/FWPU	9	10.3	67
SC-4/FWPU	6	5.8	96

No*: refer to ball number.

4. Conclusion

In this work, a novel SC/FWPU PSA was synthesized and characterized. The incorporation of SC in the polyurethane improved the thermal stability and surface roughness, resulting in increased hydrophobicity of SC/FWPU pressure sensitive adhesive. Dynamic wetting model analysis of the wettability of SC/FWPU pressure sensitive adhesive to nonpolar film suggested that the hydrophobicity of the adhesive to the nonpolar film increased with the incorporation of SC. Analyses of tack, 180° Peel strength and shear resistance of the adhesive properties of SC/FWPU adhesive to nonpolar film showed that by increasing SC contents, tack and 180° Peel strength decreased, while shear resistance increased.

Acknowledgment

We appreciate the financial support from the Science Foundation of State Key Laboratory of Structural Chemistry, China, under grant of no. 20120017.

References

[1] J.L. Zhang, D.M. Wu, D.Y. Yang, F.X. Qiu., J. Polym. Environ. 18 (2010) 128–134.
[2] H. Liu, S. Zhang, Y. Li, D. Yang, J. Hu, X. Huang, A novel perfluorocyclobutyl aryl ether-based graft copolymer via 2-methyl-1,4-bistrifluorovinyloxybenzene and styrene, Polymer 51 (22) (2010) 5198–5206.
[3] J.B. Dai, X.Y. Zhang, J. Chao, C.Y. Bai, A new core–shell type fluorinated acrylic and siliconated polyurethane hybrid emulsion, J. Coat. Technol. Res. 4 (3) (2007) 283–288.
[4] V.G. Pacios, Y. Iwata, M. Colera, J.M.M. Martinez, Influence of the solids content on the properties of waterborne polyurethane dispersions obtained with polycarbonate of hexanediol, Int. J. Adhes. Adhes. 31 (8) (2011) 787–794.
[5] P.C. Blasco, J.M.M. Martinez, I.V. Antoniac, Synthesis and characterization of polyurethane sealants containing rosin intended for sealing defect in annulus for disc regeneration, Int. J. Adhes. Adhes. 42 (2013) 11–20.
[7] L.H. Zhang, H. Zhang, J.S. Guo, Synthesis and properties of UV-curable polyester-based waterborne polyurethane/functionalized silica composites and morphology of their nanostructured films, Ind. Eng. Chem. Res. 51 (25) (2012) 8434–8441.
[8] H.C. Kuan, C.C. Ma, W.P. Chang, S.M. Yuen, H.H. Wu, T.M. Lee, Synthesis, thermal, mechanical and rheological properties of multiwall carbon nanotube/waterborne polyurethane nanocomposite, Compos. Sci. Technol. 65 (11–12) (2005) 1703–1710.
[9] Y.J. Kim, B.K. Kim, Synthesis and properties of silanized waterborne polyurethane/graphene nanocomposites, Colloid Polym. Sci. 292 (1) (2014) 51–58.
[10] L. Peng, L. Zhou, Y. Li, F. Pan, S. Zhang, Synthesis and properties of waterborne polyurethane/Attapulgite nanocomposites, Compos. Sci. Technol. 71 (2011) 1280.
[11] S. Hsiao, C.M. Ma, H. Tien, W. Liao, Y. Wang, S. Li, C. Yang, S. Lin, R. Yang, Effect of covalent modification of graphene nanosheets on the electrical property and electromagnetic interference shielding performance of a water-borne polyurethane composite, ACS Appl. Mater. Interfaces 7 (2015) 2817.
[12] F. Gao, B. Ku, S. Huang, Synthesis and characterization of bis-triethoxysilane endcapped polyurethane/urea, J. Appl. Polym. Sci. 122 (2011) 798–803.

[13] D.E. Packham, Surface energy, surface topography and adhesion, Int. J. Adhes. Adhes. 23 (2003) 437–448.
[14] S.A. Kulinich, M. Farzaneh, Effect of contact angle hysteresis on water droplet evaporation from super-hydrophobic surfaces, Appl. Surf. Sci. 255 (7) (2009) 4056–4060.
[15] Z.S. Petrovic, L. Yang, A. Zlatanic, W. Zhang, I. Javni, Network structure and properties of polyurethanes from soybean oil, J. Appl. Polym. Sci. 105 (2007) 2717–2727.
[16] V. Tomasic, I. Brnardic, H. Jenei, V. Kosar, S. Zrncevic, Combustion of active carbon as a model carbon material: comparison of non-catalytic and catalytic oxidation, Chem. Biochem. Eng. 25 (2011) 283–287.
[17] D.K. Owens, Estimation of the surface energy of polymers, J. Appl. Polym. Sci. 13 (1969) 1741–1747.
[18] S. Wu, Polymer Interface and Adhesion, M. Dekker, New York, 1982.
[19] C.W. Extrand, A thermodynamic model for contact angle hysteresis, J. Colloid Interface Sci. 207 (1998) 11–19.
[20] H.Y. Erbil, A.L. Demirel, Y. Avci, O. Mert, Transformation of a simple plastic into a super hydrophobic surface, Science 299 (2003) 1377.
[21] A.B.D. Cassie, S. Baxter, Wettability of porous surfaces, Trans. Farad. Soc. 40 (1944) 546.
[22] S.Q. Shi, D.J. Gardner, Dynamic adhesive wettability of wood, Wood Fiber Sci. 33 (2001) 58–68.